Enhancing magnetic resonance imaging tumor detection with fluorescence intensity and lifetime imaging

Ahmet Erten
University of California San Diego
Nanotumor Center
San Diego, California 92150

David Hall
Carl Hoh
University of California San Diego
Department of Radiology
3855 Health Sciences Drive
La Jolla, California 92093-0819

Hop S. Tran Cao
University of California San Diego
Moores Cancer Center
3855 Health Sciences Drive
La Jolla, California 92093-0987
and
University of California San Diego
Department of Surgery
200 West Arbor Drive, San Diego, California
92103-8220

Sharmeela Kaushal
University of California San Diego
Moores Cancer Center
3855 Health Sciences Drive, La Jolla, California
92093-0987
and
University of California San Diego
Department of Surgery
200 West Arbor Drive, San Diego, California
92103-8220

Sadik Esener
University of California San Diego
Nanotumor Center

Robert M. Hoffman
University of California San Diego
Department of Surgery
200 West Arbor Drive, San Diego, California
92103-8220
and
AntiCancer Inc.
7917 Ostrow Street
San Diego, California 92111

Michael Bouvet
University of California San Diego
Moores Cancer Center
3855 Health Sciences Drive, La Jolla, California
92093-0987
and
University of California San Diego
Department of Surgery
200 West Arbor Drive, San Diego, California
92103-8220

James Chen
Santosh Kesari
University of California San Diego
Department of Radiology
3855 Health Sciences Drive
La Jolla, California 92093-0819

Milan Makale
University of California San Diego
Nanotumor Center
San Diego, California 92150
and
University of California San Diego
Department of Radiology
3855 Health Sciences Drive
La Jolla, California 92093-0819

Abstract. Early detection is important for many solid cancers but the images provided by ultrasound, magnetic resonance imaging (MRI), and computed tomography applied alone or together, are often not sufficient for decisive early screening/diagnosis. We demonstrate that MRI augmented with fluorescence intensity (FI) substantially improves detection. Early stage murine pancreatic tumors that could not be identified by blinded, skilled observers using MRI alone, were easily identified with MRI along with FI images acquired with photomultiplier tube detection and offset laser scanning. Moreover, we show that fluorescence lifetime (FLT) imaging enables positive identification of the labeling fluorophore and discriminates it from surrounding tissue autofluorescence. Our data suggest combined-modality imaging with MRI, FI, and FLT can be used to screen and diagnose early tumors. [DOI: 10.1117/1.3509111]

Keywords: cancer detection; pancreatic cancer; orthopedic models; magnetic resonance imaging; red fluorescent protein; fluorescence intensity imaging.

Paper 10360R received Jun. 27, 2010; revised manuscript received Sep. 17, 2010; accepted for publication Sep. 21, 2010; published online Dec. 2, 2010.

1 Introduction

Early detection is critical to increase the cure rate of cancer. Unfortunately, the images provided by ultrasound, magnetic resonance imaging (MRI), and computed tomography (CT) applied alone or in combination are often inconclusive[1–10] for the identification of tumors less than 10 mm. Endoscopic ultrasonography (EUS) offers high resolution and high sensitivity but often cannot discriminate tumor tissue from inflammation, as in the case of pancreatic cancer.[5]

The present report addresses the hypothesis that MRI augmented by fluorescence intensity (FI) imaging is more likely to detect a small tumor than MRI alone.[11–15] This combined

Address all correspondence to: Milan Makale, University of California San Diego, Moores Cancer Center, 3855 Health Sciences Drive, La Jolla, California 92093-0987; E-mail: mmakale@ucsd.edu.

1083-3668/2010/15(6)/066012/6/$25.00 © 2010 SPIE

modality approach may be further augmented by fluorescence lifetime (FLT) imaging. The use of FLT imaging has recently been extended from fluorescence lifetime imaging microscopy[11] (FLIM) to whole-body imaging of rodents *in vivo*.[15] Fluorescence lifetime depends on the unique decay rate of an excited fluorophore relaxing to its ground state. Generally, the rate of decay is understood to be a sum of the rates that depopulate the excited-state of the fluorophore.[12–15] The emitted fluorescence of each fluorophore decays in a characteristic manner from radiative (photon decay) and nonradiative (nonphoton decay) events. This decay is orthogonal to FI and independent of instrument intensity acquisition settings.[16–18] FLT holds promise for tumor detection imaging, as it potentially can uniquely identify the target fluorophore. Colon tumors and skin cancers have been imaged using FLT and endoscopy.[19] However, challenges remain since FLT discrimination depends on tissue thickness, which can modify the apparent lifetime and fluorophore intensity. Experience thus far points to the necessity to develop fluorophores that have very distinct lifetimes.[19]

The primary aim of this study is to improve magnetic resonance (MR) detectablity of small tumors with FI and possibly FLT imaging.

To demonstrate the potential utility of augmenting MRI with FI, pancreatic tumors were orthotopically implanted in athymic (nu/nu) mice, and the tumor was imaged with multiple modalities at different stages of growth. FLT imaging was also attempted to determine if it could confirm or enhance the effects of FI. For each mouse, we acquired MRI, FI, and FLT images and compared them in terms of tumor detection. FI acquisition used a continuous wave (cw) system with a halogen lamp CCD camera with direct illumination as well as a time-domain (TD) system with a pulsed laser and a time-correlated single-photon-counting (TCSPC) photomultiplier tube (PMT) detector with raster scanning.

The pancreatic tumors were imaged with multiple modalities at different stages of growth. Our previous studies have shown that tumors arising from orthotopically-implanted pancreatic tumor cells in nude mice can be imaged with MRI as well as planar FI imaging.[20] For each mouse, we acquired MRI, FI, and FLT images and determined if FI and FLT could augment MRI for the detection of very small tumors.

2 Materials and Methods

2.1 *Pancreatic Tumor Model*

2.1.1 *Animal subjects*

Athymic male nu/nu nude mice were maintained in a barrier facility under pathogen-free conditions. All surgical procedures and intravital imaging were approved by the University of California San Diego (UCSD) institutional animal care and use committee (IACUC). In addition, all research was conducted in accordance with approved UCSD Animal Care Program protocols, and within the guidelines of the National Institutes of Health's *NIH Guide for the Care and Use of Animals.*

2.1.2 *Orthotopic tumor implantation*

Twelve mice were anesthetized and placed in the right decubitus position. The left lateral flank was sterilized using Betadine®. A small transverse incision was made through the skin and peritoneum overlying the spleen. The pancreas was then gently exposed. A 20-μL Hamilton syringe (Hamilton Co., Reno, Nevada) was used to inject the pancreatic tail with a human pancreatic cancer cell line that stably expressed red fluorescent protein [MiaPaca-2 RFP, 10^6 cells in 2.5 μL RPMI + matrigel (1:1)]. The peritoneum and skin were then closed using 6-0 Ethibond® suture (Ethicon, Somerville, New Jersey).

2.2 *Imaging*

2.2.1 *MRI*

Four mice, at each of three time points, which were 5, 7, and 12 days after implantation, were anesthetized with 1.5% isoflurane. They received intravenous gadolinium contrast agent (Magnevist), and were placed within a bird-cage-type of mouse body coil. A respiratory bellows was used to monitor respiration and a nose cone delivered the inhalation anesthetic. The mouse was positioned at the isocenter of the scanner magnet, and the bore was warmed to 36°C. A fast 3-D localizer scan was performed, followed by T1-weighted 3-D structural scans. The 3-D scan acquisition time was 1357 s, the acquisition matrix was 256×128, repetition time (TR) = 885.7, the time to echo (TE) = 10 ms, averages = 6, and the slice thickness was 0.6 mm. The 3-D data sets were reconstructed and saved in standard DICOM (digital imaging and communications in medicine) format.

2.2.2 *FI and FLT imaging*

The Advanced Research Technologies (ART) Optix-MX2® imaging system was used to acquire both the intensity and the time domain-based fluorescence images. This apparatus includes four pulsed lasers (picosecond pulse, 80-MHz duty cycle), eight filters, and a TCSPC PMT for TD detection. A brightfield image was acquired first, followed by TD fluorescence detection from which FI and FLT images were obtained. The FLT image acquisition times ranged between 2 and 7 min, depending on the size of region of interest. The Optix-MX2® images were acquired with euthanized mice that were placed supine. The image data were saved directly on a PC for later processing.

2.2.3 *Confirmation of tumors in each subject*

To determine whether each mouse had developed a tumor, and to provide a record of tumor location, the mice were euthanized and then laparotomized. The pancreatic tumor was exposed by blunt dissection. Direct brightfield and fluorescence imaging of the exposed tumor provided a record of the tumor for each mouse. FI images were acquired with an Olympus OV100 Small Animal Imaging System (Olympus Corp., Tokyo, Japan). This instrument was used because of its ability to magnify over a large range. The OV100 included a DP70 CCD camera (Olympus Corp., Tokyo, Japan), with a range of lens magnifications [$0.14 \times (63 \times 47$ mm imaging area) to $16 \times (0.6 \times 0.45$ mm)].

2.3 *Image Data Processing*

2.3.1 *Image coregistration and fusion*

Coronal MRI volume image slices were coregistered with the Optix® FI/FLT images using a custom program prepared with IDL software (ITT Visual Solutions, Boulder, Colorado). Registration was based on the mutual information criteria. Briefly, the

3-D MR data volume of the mouse torso was coregistered to the 2-D fluorescence image by a computer algorithm that iteratively rotated and translated the MR volume in three rotational and three translational parameters. Initially, regions of interest were drawn to isolate the anatomic regions to be matched and then the mutual information criteria between the two images were maximized. During each iteration, the 3-D MR data volume was reprojected into a 2-D image prior to determining the mutual information criteria. The mutual information criteria incorporated in the software has a maximum at the best registration for a given set of images. This maximum value varies depending on the content of the two images. The final coregistered MR tomographic set was used for tumor identification. The MR volume slice that most closely corresponded in terms of z to the FI/lifetime image used for coregistration was selected and alpha blended with the fluorescence image to create a fused image. The opacity of the FI image was adjusted to permit simultaneous viewing of its corresponding MR. The FI image was processed prior to alpha blending, so that only the lifetime pixels corresponding to the fluorophore were visible.

2.3.2 *Assessing tumor detection with MRI, FI, and FLT*

The images from the MRI volumes were assembled into panels for each mouse with an identification code. Subsequently, two trained observers, one an oncologist and the second a radiologist, skilled in oncology screening, were asked to determine which mice had identifiable tumors in the pancreas, and then tabulate their assessments. These two evaluators were not informed as to the stage or age of the tumor implantation in each mouse.

3 Results

3.1 *Tumor Detection by MRI Alone*

MRI enabled detection of tumors for all four of the most advanced tumors. These were imaged at 12 days from implantation (Table 1) and were over 1.0 cm in diameter. For the 7-day group, however, two of the four tumors were not considered detectable by one of the expert readers, and both readers had difficulty detecting tumors at the 5-day time point (smallest tumors). With both readers, only one positive identification at 5 days was tabulated, and this was considered questionable. Figure 1(a) left panel is a T1-weighted gadolinium-enhanced MR image slice of a mouse bearing a 5-day pancreatic tumor, which was not detectable. In contrast, the tumors at 7 and 12 days, middle and right panels, respectively, both were visible by MRI. Figure 1(b) shows a fluorescence image of the same subject in the Fig. 1(a) left panel, after laparotomy and dissection, and the tumor is clearly highlighted confirming its presence.

3.2 *Tumor Detection by MRI and FI Together*

FI acquired by photon counting with scanning laser illumination and a PMT detector on the Opitx-MX2® system, supported tumor detection (Table 1). For all 12 mice, MRI unambiguously detected 6/12 tumors, for reader 2 the worst case, while FI alone detected 10/12, and combined modality detection was 12/12. MRI versus FI did not differ significantly, but MRI alone versus combined modality (MRI + FI) differed according to Fisher's exact probability ($p = 0.014$). FLT did not contribute significantly to detection.

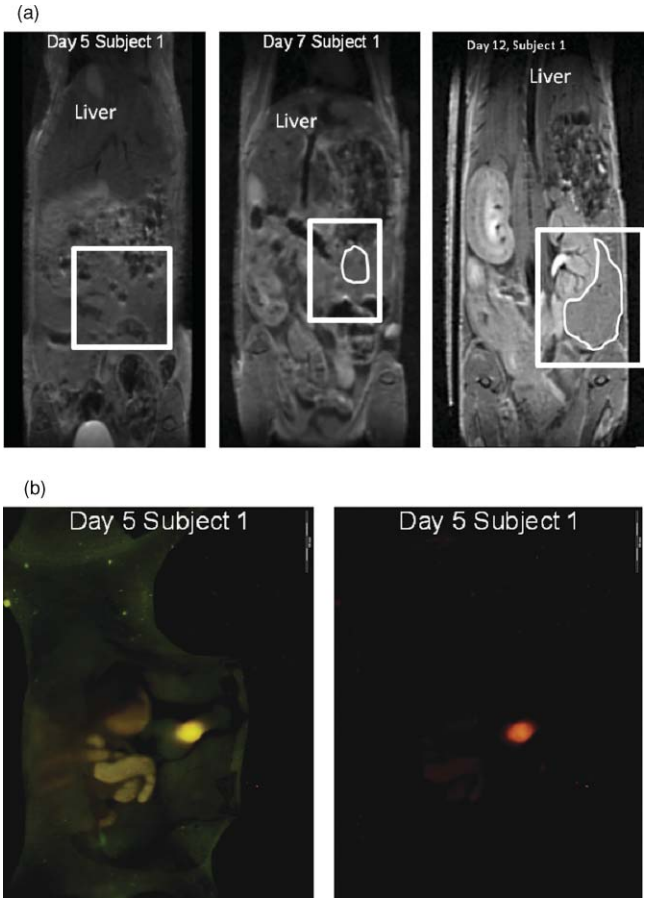

Fig. 1 (a) Images are T1-weighted MRI image slices acquired at 5 days (left panel), 7 days (middle panel), and 12 days right panel) after orthotopic pancreatic tumor implantation. The tumor is visible at day 7 and at day 12, but is not apparent at day 5, even though later dissection proved its existence. The white squares indicate the location of the pancreas, and the tumor is outlined where it is visible. The liver is shown to provide orientation. Each view is of a supine animal from above. The images indicate the difficulty associated with discerning the presence of a very small tumor with MR alone. (b) Dissection of day 5 subject [MR image is shown in (a) left panel], the tumor green channel FI (left) and red FI (right) were imaged with the OV100. The red fluorescent protein (RFP) labeling spills into the green channel (530/50 filter), so that the resultant autofluorescence provides some anatomical-positional context, while in the left panel only the red fluorescence from the RFP label is detectable though the 598/55 bandpass filter. Both images confirm that a tumor was present. This tumor was not detectable with MRI.

3.3 *Tumor Detection by FLT and FI Together*

Figure 2, left panel, shows the same mouse as in Fig. 1(a); the tumor presence is indicated by the fluorescence hotspots near the left flank, but other intensely fluorescent sites are present. These likely arose from vegetable food matter in the gut. Figure 2, middle panel, shows a cleanly delineated area of the gated FLT map near the left flank in the same approximate areas as a candidate FI hotspot. In this image, only pixels from the FLT associated with the RFP fluorophore were displayed. The tumor is separated from the surrounding tissue. Figure 2, right panel, is a fluorescence image acquired after laparotomy

Table 1 Tumor detection with different imaging modalities applied alone and in combination.

	Imaging Modality				
Time point (days)	MRI Reader 1	MRI reader 2	FI (PMT-Laser Scanning)	Combined MRI + FI	Confirmed by FLT
5 subject 1	ND	ND	**Det**	**Det**	Yes
5 subject 2	ND	ND	**Det**	**Det**	Yes
5 subject 3	ND	ND	**Det**	**Det**	No
5 subject 4	Det-AMB	**Det**	**Det**	**Det**	Yes
7 subject 1	**Det**	**Det**	**Det**	**Det**	Yes
7 subject 2	**Det**	**Det**	ND	**Det**	No
7 subject 3	**Det**	ND	**Det**	**Det**	No
7 subject 4	**Det**	ND	**Det**	**Det**	No
12 subject 1	**Det**	**Det**	ND	**Det**	No
12 subject 2	**Det**	**Det**	**Det**	**Det**	Yes
12 subject 3	**Det**	**Det**	**Det**	**Det**	Yes
12 subject 4	**Det**	**Det**	**Det**	**Det**	No

Det, detected; Det-AMB, detected but not confirmed; ND, not detected.

and dissection, confirming the presence of the tumor. The use of FLT with FI confirmed the presence of the RFP fluorophore in three of four of the smallest (5 day) tumors.

The top image on the left of Fig. 3 shows tumor RFP FI and abdominal autofluorescence FI. The lower image acquired from a different subject indicates tumor FI and two intestinal FI sites. The FLT graph was prepared using data for all sites in the two images. Note that the RFP FLT decay curves for tumors from two different subjects are virtually identical (upper curves), and that the intestinal autofluorescence FLT decay curves (lower) are also the same but clearly different from the RFP curves.

3.4 *Coregistration of MRI, FI, and FLT*

Coregistration of the MRI image slices with gray-scale optical, FI, and FLT images, enabled the tumor to be highlighted within its anatomical context, as shown in Fig. 4 (left and right panels). The FLT decay image in particular (Fig. 4, right panel), where nontumor FLT decay pixels were set to zero, clearly delineated the tumor within its anatomical environment, which was described by the fused MRI and gray-scale (optical) images of the mouse torso.

4 Discussion

The combination of MRI along with laser-scanning, offset-illumination FI imaging markedly improved the detection of small tumors. The addition of FLT mapping further augmented this enhancement in a significant proportion of cases, allowing discrimination of tumor tissue from surrounding host tissue. The fluorescence detection process can be viewed as comprising two steps: (1) detection of fluorophores associated with the target and (2) discrimination of the target fluorescence from surrounding autofluorescence. Fluorescence emission lifetime decay, owing to its independence from intensity, addresses the second part of the process.

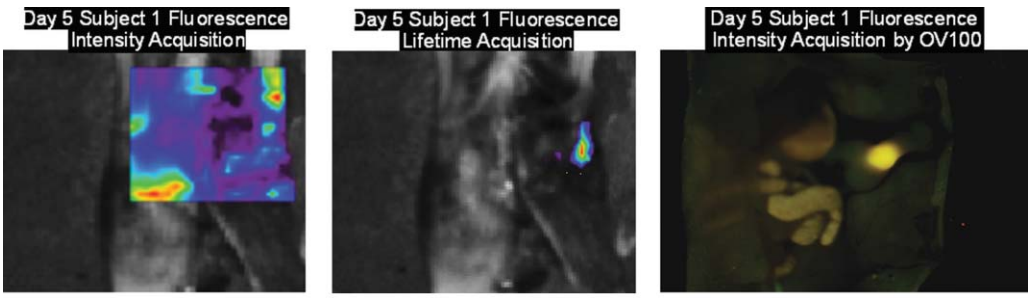

Fig. 2 (a) The FI and (b) the corresponding gated FLT decay map (Optix-Mx2). (c) The FI image acquired after laparotomy and dissection to directly expose the tumor.

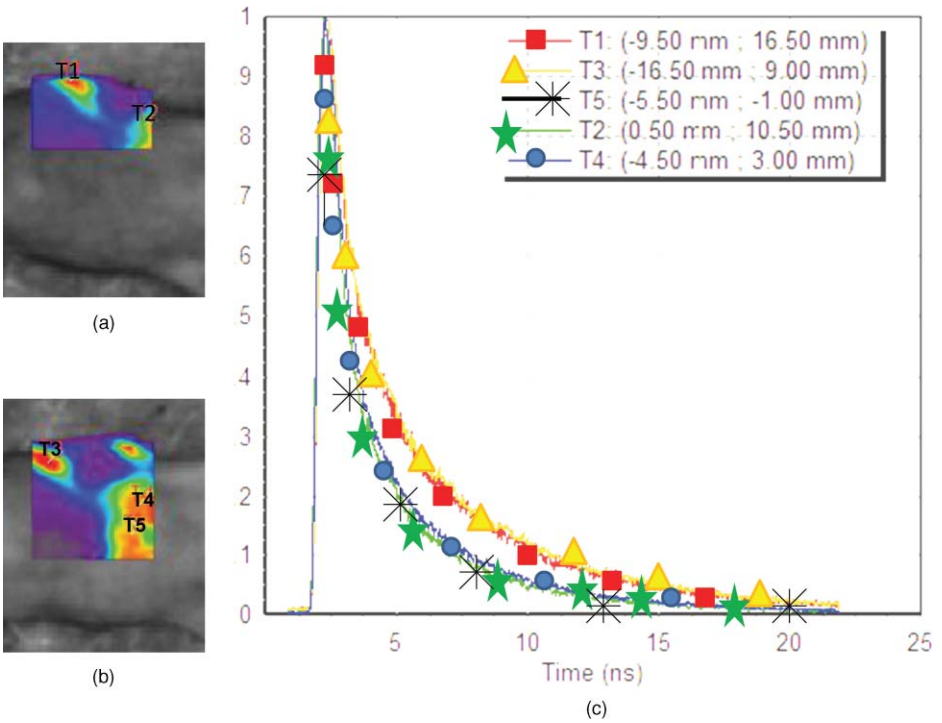

Fig. 3 Image panels (Optix-MX2).(a) The FI image with a labeled tumor (T1) and an intestinal auotfluorescence (T2) hotspot due to vegetable food in the intestinal lumen. (b) The FI image for another subject and the tumor fluorescence is labeled T3. Two intestinal autofluorescent sites are visible in this image, labeled T4 and T5. (c) Graph panel (Optix-MX2) shows the FLT curves from pixels from all five sites labeled in the images of 4a and b. Note that the tumor FLT curves are virtually identical for the tumor tissue from different subjects (T1 and T3) and that the intestinal autofluorescence (T2, T4, and T5), is the same between subjects. The tumor FI decay curves are distinct from the autofluorescence FLT decay curves.

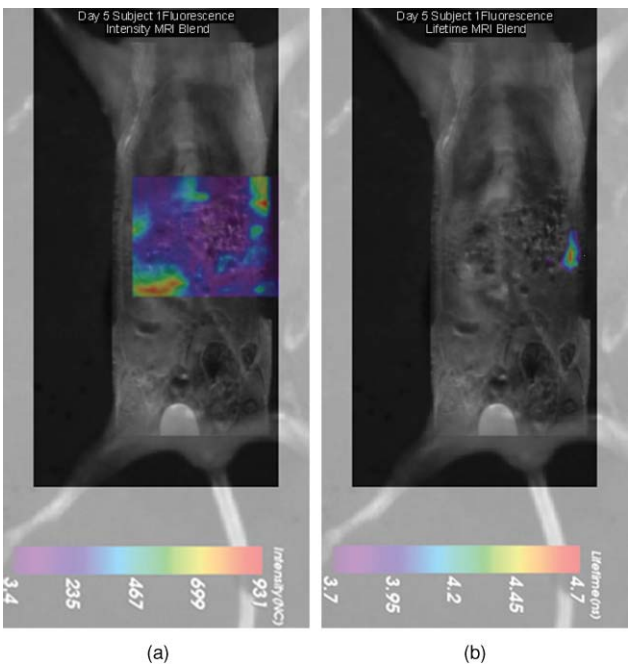

Fig. 4 Illustration that the MRI and FLT modalities can be combined. (a) The FI image (Optix-MX2) and mouse gray-scale image of a 5-day tumor coregistered with and displayed on a corresponding MRI acquisition slice. (b) A FLT image (Optix-MX2) that has been gated so that all pixels not associated with the fluorophore FLT are set to zero. The FLT image and the gray-scale mouse image have been morphed to match the corresponding MRI slice, and all three images are displayed together.

In this study, each mouse served as its own control whereby the presence of a tumor was confirmed by dissection and direct observation after it had been imaged. We found no "false positives," i.e., incorrectly calling a tumor to be present on MRI or combined modality when in fact one was not present. Since these tumors were entirely confined to the pancreas, especially in the early time points when the tumors were extremely small, normal tissue autofluorescence was not different between tumor-bearing and non-tumor-bearing mice. The intestines, rather than the pancreas, were the main source of autofluorescence due to their food content.

In many instances, the tumor FLT was discriminated cleanly from surrounding tissues, but in other instances, the weaker intensity of the fluorescence signal did affect separation on the basis of lifetime decay. This highlights one difficulty inherent in FLT imaging, which is that a very large number of decay curves must be tediously analyzed to separate the fluorophore of interest.[21]

The best solution to minimize interference from autofluorescence when the fluorophore signal is expected to be weak, for example, due to sparse labeling of a tumor, is to use a labeling fluorophore with the longest lifetime possible. Unfortunately, lifetime has an inverse relationship with another desirable fluorophore attribute, namely, long emission wavelength to reduce scatter and improve tissue penetrance. Most organic fluorophores that have longer wavelength emissions also have short fluorescence emission lifetimes.[17] An exception are quantum dots, which emit long wavelengths and at the same time have a relatively long fluorescence decay.[15] An example is Qdot800,

which emits at 800 nm, a very long wavelength that enables deeper imaging, and it has a very long FLIM decay of 20 ns, which is ideal. However, Qdot800 is difficult to link to biological molecules such as targeted antibodies, and one of its components is cadmium metal, which is toxic. Therefore, new labeling fluorophores need to be developed that are optimized in terms of emission wavelength, fluorescence lifetime, and toxicity profile.

In summary, this paper demonstrated that combined modality imaging of the mouse pancreatic tumor model using MRI along with FI, augmented tumor detection over MRI alone. Future work will address the clinical potential of this approach in particular with fluorescence endoscopy.

Future studies will involve comparision of MRI to an injected fluorophore, to account for tumor delivery issues related to the targeted fluorophore. This early study used cells expressing a fluorophore to avoid complexities such as the distribution of the fluorophore, the kinetics of tumor accumulation of the fluorophore, extravasation into normal tissues, and concentration issues. We then sought to demonstrate that with optical methods it is feasible to augment MRI with the best-case scenario. A much more comprehensive study comparing MRI to an injected fluorophore will be carried out in the future. This study, however, indicates that MRI can be augmented by FI, which has implications for clinical application for early detection of cancer.

Acknowledgments

The authors wish to acknowledge the excellent editorial assistance of Ms. Charlene M. Cooper, and the expert imaging assistance provided by Mr. Salman Farshchi-Haydari. This work was in part funded by the National Cancer Institute Grant No. CA109949 and the American Cancer Society Grant No. RSG-05-037-01-CCE (to M.B.), T32 training Grant No. CA121938 (to H.S.T.C.), National Cancer Institute Grant No. CA132971 (to M.B. and AntiCancer Inc.), National Institutes of Health (NIH) Grant No. S10 RR22599-01A1 (to D.J.H) and NIH Grant No. P50 CA128346-01A1.

References

1. M. Anzidei, A. Napoli, F. Zaccagna, P. Di Paolo, C. Zini, B. Cavallo Marincola, D. Geiger, C. Catalano, and R. Passariello, "Diagnostic performance of 64-MDCT and 1.5-T MRI with high-resolution sequences in the T staging of gastric cancer: a comparative analysis with histopathology," *Radiol. Med.* **114**, 1065–1079 (2009).
2. D. V. Sahani, Z. K. Shah, O. A. Catalano, G. W. Boland, and W. R. Brugge, "Radiology of pancreatic adenocarcinoma: current status of imaging," *J. Gastroenterol. Hepatol.* **23**, 23–33 (2008).
3. Y. L. Bronstein, E. M. Loyer, H. Kaur, H. Choi, C. David, R. A. DuBrow, L. D. Broemeling, K. R. Cleary, and C. Charnsangavei, "Detection of small pancreatic tumors with multiphasic helical CT," *AJR Am. J. Roentgenol.* **182**, 619–623 (2004).
4. M. B. Sheridan, J. Ward, J. A. Guthrie, J. A. Spencer, C. M. Craven, D. Wilson, P. J. Guillou, and P. J. Robinson, "Dynamic contrast-enhanced MR imaging and dual-phase helical CT in the preoperative assessment of suspected pancreatic cancer: a comparative study with receiver operating characteristic analysis," *AJR Am. J. Roentgenol.* **173**, 583–590 (1999).
5. P. Michl, S. Pauls, and T. M. Gress, "Evidence-based diagnosis and staging of pancreatic cancer," *Best Pract. Res. Clin. Gastroenterol.* **20**, 227–251 (2006).
6. D. W. Roberts, P. A. Valdés, B. T. Harris, K. M. Fontaine, A. Hartov, X. Fan, S. Ji, S. S. Lollis, B. W. Pogue, F. Leblond, T. D. Tosteson, B. C. Wilson, K. D. Paulsen, "Coregistered fluorescence-enhanced tumor resection of malignant glioma: relationships between delta-aminolevulinic acid-induced protoporphyrin IX fluorescence, magnetic resonance imaging enhancement, and neuropathological parameters," *J. Neurosurg.* (2010), Epub ahead of print.
7. P. Zou, S. Xu, S. P. Povoski, A. Wang, M. A. Johnson, E. W. Martin Jr., V. Subramaniam, R. Xu, and D. Sun, "Near-infrared fluorescence labeled anti-TAG-72 monoclonal antibodies for tumor imaging in colorectal cancer xenograft mice," *Mol. Pharm.* **6**, 428–440 (2009).
8. R. C. Liu and L. W. Traverso, "Diagnostic laparoscopy improves staging of pancreatic cancer deemed locally unresectable by computed tomography," *Surg. Endosc.* **19**, 638–642 (2005).
9. M. Loning, H. Diddens, W. Kupker, K. Diedrich, and G. Huttmann, "Laparoscopic fluorescence detection of ovarian carcinoma metastases using 5-aminolevulinic acid-induced protoporphyrin IX," *Cancer* **100**, 1650–1656 (2004).
10. S. Faiss, J. S. Lewin, S. G. Nour, M. Zeitz, J. L. Duerk, F. K. Wacker, "Endoscopically inserted endoluminal receiver coil for high-resolution magnetic resonance imaging of the pancreas: initial results in an animal model," *Gastrointest. Endosc.* **57**, 106–110 (2003).
11. T. M. Jovin, D. S. Lidke, and E. A. Jares-Erijman, "Fluorescence resonance energy transfer (FRET) and fluorescence lifetime imaging microscopy (FLIM)," in *From Cells to Proteins: Imaging Nature across Dimensions*, V. Evangelista et al. Eds., pp. 209–216, The Netherlands: Springer, 2005.
12. R. Cubeddu, D. Comelli, C. D'Andrea, P. Taroni, and G. Valentini, "Time-resolved fluorescence imaging in biology and medicine," *J. Phys. D Appl. Physi.* **35**, R61–R76 (2002).
13. P. J. Tadrous, "Methods for imaging the structure and function of living tissues and cells: 2. Fluorescence lifetime imaging," *J. Pathol.* **191**, 229–234 (2000).
14. D. Elson, J. Requeio-lsidro, I. Munro, F. Reavell, J. Siegel, K. Suhling, P. Tadrous, R. Benninger, P. Lanigan, J. McGinty, C. Talbot, B. Treanor, S. Webb, A. Sandison, A. Wallace, D. Davis, J. Lever, M. Neil, D. Phillips, G. Stamp, P. French, "Time-domain fluorescence lifetime imaging applied to biological tissue," *Photochem. Photobiol. Sci.* **3**, 795–801 (2004).
15. D. J. Hall, U. Sunar, S. Farshchi-Heydari, and S. H. Han, "In vivo simultaneous monitoring of two fluorophores with lifetime contrast using a full-field time domain system," *Appl. Opt.* **48**, D74–D78 (2009).
16. A. May, S. Bhaumik, S. S. Gambhir, C. Zhan, and S. Yazdanfar, "Whole-body, real-time preclinical imaging of quantum dot fluorescence with time-gated detection," *J. Biomed. Opt.* **14**, 060504 (2009).
17. S. W. Botchway, M. Charnley, J. W. Haycock, A. W. Parker, D. L. Rochester, J. A. Weinstein, and J. A. Williams, "Time-resolved and two-photon emission imaging microscopy of live cells with inert platinum complexes," *Proc. Natl. Acad. Sci. U. S. A.* **105**, 16071–16076 (2008).
18. W. J. Akers, M. Y. Berezin, H. Lee, and S. Achilefu, "Predicting *in vivo* fluorescence lifetime behavior of near-infrared fluorescent contrast agents using *in vitro* measurements," *J. Biomed. Opt.* **13**, 054042 (2008).
19. M. Y. Berezin and S. Achilefu, "Fluorescence lifetime measurements and biological imaging," *Chem. Rev.* **110**(5), 2641–2684 (2010).
20. M. Bouvet, J. Spernyak, M. H. Katz, R. V. Mazurchuk, S. Takimoto, R. Bernacki, Y. M. Rustum, A. R. Moossa, and R. M. Hoffman, "High correlation of whole-body red fluorescent protein imaging and magnetic resonance imaging on an orthotopic model of pancreatic cancer," *Cancer Res.* **65**, 9829–9833 (2005).
21. S. Pelet, M. J. Previte, L. H. Laiho, and P. T. So, "A fast global fitting algorithm for fluorescence lifetime imaging microscopy based on image segmentation," *Biophys. J.* **87**(4), 2807–2817 (2004).